Atomistic structure of oxide nanoparticles supported on an oxide substrate

Dean C. Sayle,[1,*] James A. Doig,[1] S. Andrada Maicaneanu,[1] and Graeme W. Watson[2]
[1]*Department of Environmental and Ordnance Systems, Cranfield University, Royal Military College of Science, Shrivenham SN6 8LA, Swindon, United Kingdom*
[2]*Department of Chemistry, Trinity College, Dublin 2, Ireland*
(Received 5 November 2001; revised manuscript received 21 February 2002; published 7 June 2002)

The atomistic structures of SrO ($15\times15\times2.2$ nm), CaO ($14\times14\times2$ nm), and MgO ($12\times12\times2$ nm) nanoparticles, supported on BaO(001) and synthesized using a simulated amorphization and recrystallization strategy, are presented. The SrO and CaO exhibit cubic ''slab'' morphologies in contrast to the MgO nanoparticle, which comprises various misaligned interconnecting crystallites. The lattice misfit was found to have a profound influence on the structure of the nanoparticles. The SrO nanoparticle (-7% misfit) was found to lie coherent with respect to the substrate across the entire area covered by the SrO. Conversely, only small regions of the CaO were found to be coherent with the BaO substrate (-15% misfit), with screw-edge dislocations located at regions where the ions became misaligned. The MgO nanoparticle (-31% misfit) exhibited no regions of coherence with respect to the underlying BaO substrate. Defects (vacancies and substitutionals) and defect clusters including voids were also identified for each system and act to help reduce locally the lattice misfit thereby enhancing the stability. Specifically, the results indicate that as the lattice misfit associated with the system increases, so the interfacial layer of the substrate becomes more defective. Arguments, based on the results of the study, are presented, which suggest that the area of the nanoparticle in contact with the substrate is linked with the critical thickness to dislocation evolution for a particular system. That the limitations of periodic boundary conditions can be eliminated when simulating nanoparticles compared with thin films, which cover completely the substrate material, is discussed.

DOI: 10.1103/PhysRevB.65.245414 PACS number(s): 68.55.Jk; 61.43.Bn; 61.43.Er

I. INTRODUCTION

The influence of supporting a material on a lattice-mismatched substrate can have a profound influence on the chemical, physical, and mechanical properties of the material,[1–3] as the material responds structurally to the lattice misfit associated with the system and the interfacial interactions when supported. These include changes in morphologies and hence the particular surfaces exposed,[4,5] the evolution of structural features, such as grain-boundaries,[6–8] dislocation arrays,[9] defects[10,11] (substitutionals, vacancies, interstitials including defect clustering) and epitaxial configurations.[5] In addition, the method and conditions of fabrication play a central role in controlling the structure and hence properties of the supported material. Such phenomena have been exploited widely to improve the effectiveness of particular devices and have spawned new applications, spanning, for example, electronics, optical, catalysis, sensors, and recording media.

The physical and chemical properties of a material can also be changed dramatically when the size of the particles is reduced to the nanometer scale.[12–15] Clearly, to understand and exploit the remarkable properties of such nanoparticles requires a detailed knowledge of their microstructure and while this is currently an area of intense and growing interest[16–21] it is difficult to elucidate the structure of supported nanoparticles at the atomic level experimentally.[1] Conversely, where simulation has proved difficult previously owing to the complexity in spanning various length scales (atomic to macroscale) it is arguably ideally suited to explore systems, which exist at the nanometer scale. Indeed, such systems can be treated with considerable rigor[16] as each atom comprising the nanoparticle can be treated explicitly without imposing periodic boundary conditions or resorting to continuum methods. Accordingly, in this study, we employ atomistic simulation techniques that we developed previously to investigate thin films, to explore the influence of supporting nanoparticles on a substrate material. The aim of this present study is to generate models of supported oxide nanoparticles, which will provide information pertaining to nanoparticle morphologies and exposed surfaces, epitaxial relationships, defects, dislocations and grain boundaries, and the influence of the substrate material and associated lattice misfit on such structural modifications. At present, it is extremely difficult if not intractable to elucidate such information experimentally. Accordingly, simulation is well positioned as a complementary technique. Conversely, experimental data on supported oxide nanoparticles, which includes atomistic detail to compare with our simulations are sparse.

In a previous study, we investigated the structural features associated with supporting a small ($125\times125\times20$ Å) MgO particle on a BaO oxide substrate.[22] Here, we extend this study by considering three oxides SrO, CaO, and MgO supported on BaO(001) as models to help ascertain the influence the lattice misfit may have on the structure of oxide nanoparticles supported on an oxide support, which has a *higher* lattice parameter. Specifically, the three systems are associated with lattice misfits of -7, -15, and -31% for SrO, CaO, and MgO, respectively. The percent misfit F is given by

$$100\times\left(\frac{a_{\mathrm{nano}}-a_{\mathrm{sub}}}{a_{\mathrm{sub}}}\right), \tag{1}$$

where a_{nano} and a_{sub} are the lattice parameters of the nanoparticle and substrate, respectively.

In contrast to previous simulations on fully covered thin films[23] using an analogous methodology, the simulations on nanoparticles, presented here, do not suffer from limitations associated with employing periodic boundary conditions. For example, with completely covered thin films, the structural connection of the periodic repeats must be seamless to maintain continuity with neighboring images, which will necessarily introduce artificial features within the simulation.

To ensure continuity has proved difficult to overcome[24,25] especially where the simulation cell is constructed ''by hand'' as one needs to determine how the ions comprising the thin film are arranged with respect to the underlying substrate to ensure that the system is lattice matched. In addition, one needs also to include all the structural features associated with a lattice-mismatched system including grain boundaries, dislocation arrays, defects (comprising vacancies, interstitials, and substitutionals), defect clustering, and epitaxial relationships, all of which must be integrated to ensure seamless continuity of the thin film with respect to the periodic boundary conditions (PBC's).

One enabling development, a simulated amorphization and recrystallization methodology, has facilitated the structural evolution of thin films (and include grain boundaries, dislocations, and defects) in response solely to the lattice misfit and interfacial interactions. This methodology has been applied successfully to generate models for CaO, SrO, and BaO thin films supported on an MgO(001) substrate,[23] MgO/BaO(001),[26] MgO, and BaO supported on $SrTiO_3(001)$ (Ref. 27) and $CeO_2/ZrO_2(111)$.[28,29] In addition, the methodology ensures that the continuity between periodic images is resolved implicitly during the structural evolution of the thin film.[30] However, such simulations still remain subject to limitations arising from imposing PBC's upon the system. For example, the sum of the Burgers vectors (resolved parallel with the interfacial plane) for all the dislocations within the simulation cell must equate to an integer number of unit cells. This limitation can be offset partially by increasing the size of the simulation cell and thereby enabling a higher number of dislocations to evolve within the simulation cell[24] and preventing the simulation from evolving dislocations somewhat artificially. Conversely, in simulating nanoparticles, there are no interactions between neighboring nanoparticles and issues pertaining to ensuring continuity and the associated limitations, relating to the quality of the resulting models, do not arise.

II. METHODOLOGY

In this section we describe the force field, which we have used to describe the interactions within the materials considered, the simulation codes and how they can be used to perform surface calculations, and, finally, the basic mechanism underlying the operation of the simulated amorphization and recrystallization procedure.

A. Potential models

The reliability of any atomistic simulation rests ultimately with the potential parameters.[31] Our calculations are based on the Born model of the ionic solid in which the ions interact via long-range Coulombic interactions, calculated using the Ewald summation[32] and short-range parametrized interactions. In this study we have employed the potential parameters of Lewis and Catlow[33] with the additional approximation of the rigid ion model, imposed to reduce the computational expense. The potential parameters have been extensively employed previously to model structures, which have nonoptimal geometries, with good correlation to experiment.[3] These include interfacial structures,[34] surface and interfacial defects,[35,36] dislocations,[9,37] and grain boundaries.[26] We suggest therefore that the potential parameters are well suited to explore supported metal-oxide thin films, which may include many structural defects.

B. Simulation codes

In this study, we employ the DL_POLY code[38] to perform the dynamical simulations. Since this code utilizes three-dimensional periodic boundary conditions, the surface of the BaO substrate is simulated using a periodic array of slabs with a void introduced perpendicular to the interfacial plane to represent the vacuum above the surface of the thin film. The size of the void is, of course, suitably large to ensure that the interactions between slabs are negligible. The SrO, CaO, or MgO nanoparticles are then placed on top of the BaO substrate with a minimum distance between neighboring nanoparticles of 80 Å to eliminate (artificial) interactions between the nanoparticle and its periodic images.

We employ a standard two-region approach.[37] Region I contains the MO (M = Sr, Ca, or Mg) nanoparticle and one repeat unit of the underlying BaO support and ions within this region are allowed to move within the dynamical simulation, while ions in region II (three BaO repeat units thick) are held fixed to reproduce the potential of the bulk lattice on region I.

The reason for using DL_POLY [codes using two-dimensional (2D) periodicity are available[39]], is that it offers a considerable speed advantage for our particular application. (We have found previously[9,24] that simulating interfaces using an amorphization and recrystallization methodology with either 2D or 3D periodic boundary conditions gave rise to equivalent results.) In particular, for simulating supported nanoparticles, the interfacial area must be large to ensure that the nanoparticle does not interact with its images within the periodic boundary conditions. Moreover, the structural modifications, such as dislocation networks and grain boundaries that evolve as the overlying material responds to the misfit strain, are large and the size of the simulation cell must be chosen to suitably accommodate such features. Accordingly, the vector introduced perpendicular to the surface to generate the vacuum above the thin film, while being sufficiently large to prohibit any artificial interactions between the system and its periodic images, is also our smallest vector, which facilitates a very efficient 3D simulation. Many simulations of surfaces performed using 3D codes are inefficient owing to the large sampling of reciprocal lattice vectors perpendicular to the surface in the Ewald sum compared with the other two directions. In addition, by performing the dynamical simula-

tions on a parallel computer (typically such calculations require 14 days using 16 processors of an Origin 2000), we benefit also from the efficiency of the DL_POLY code when run in parallel.

All simulations were performed within the *NVE* ensemble: constant number of particles, constant volume, and constant energy with instantaneous velocity scaling to the simulation temperature used throughout. This is to prevent the rapid and large build up of excess kinetic energy as the nanoparticle evolves from the highly strained initial configuration, via an amorphous transition to a crystalline phase with reduced strain.

C. Amorphization and recrystallization

The very short time scales accessible to atomistic dynamical simulations (typically a nanosecond) is a major limitation with the technique. Consequently, for highly crystalline materials, such as MgO, where ionic migration is slow, dynamical simulation is not appropriate to explore the energy barriers for migration since no migration would be observed within the time scales accessible. Conversely, central to the methodology employed in this present study, is that for an amorphous material the ions will have a much higher mobility and can therefore migrate more quickly (within the time scales available) compared with the analogous crystalline solid. This simulation technique therefore involves forcing the overlying material to undergo, under dynamical simulation, a controlled amorphization. This allows the ions to evolve and assemble into an appropriate (low-energy) configuration, which would not be possible by applying dynamical simulation to crystalline materials. The prolonged application of dynamical simulation to this amorphized nanoparticle results in its recrystallization together with the evolution of structural features relating to the accommodation of the associated lattice misfit such as grain boundaries, dislocations, defects, and reduced interfacial ion densities. The amorphization and recrystallization strategy provides therefore a mechanism for overcoming, in part, the considerable (time) limitation associated with dynamical simulation. The final nanoparticle structure is governed solely by the interfacial interaction and lattice misfit associated with the system rather than the (artificial) starting configuration.

The basic approach is to control the transformation to an amorphous state by use of an initial strain on the nanoparticle structure, an appropriate temperature, and velocity scaling. The subsequent application of high-temperature dynamical simulation to the system then results in its amorphization. Essentially, the initial strain is sufficient to effect the amorphous transition and the system is then allowed to evolve without further constraint. Further details of the technique can be found elsewhere.[24] Here we induce amorphization by initially expanding the structure of the nanoparticle (tension induced amorphization), which is perhaps more appropriate than amorphization induction via compression since the former will result in a contraction of the supported nanoparticle as it amorphizes. Consequently, the minimum distance between the nanoparticle and its periodic images is more easily controlled. In addition, one must ensure that the nanoparticle does not melt as this is likely to result in the complete spreading of the nanoparticle over the surface of the underlying support. Accordingly, the dynamical simulation is performed at a sufficiently high temperature to maximize ionic mobility without resulting in melting and was monitored using mean square displacements.

In previous studies, we have found that the degree of compression/tension imposed upon the overlying oxide to induce amorphization can prove critical to the successful recrystallization of the material.[40] For example, if the compression is too low the oxide fails to amorphize and no structural features evolve. Essentially, the ions comprising the thin film are not sufficiently mobile to move into low-energy configurations owing to the high-energy barriers for ionic migration; rather they vibrate about their respective lattice positions. At higher yet still insufficient compression, the oxide may indeed undergo an amorphous transition (as monitored using ion density functions, radial distribution functions, and simple inspection of the ion positions) although during prolonged dynamical simulation, the oxide fails to recrystallize or alternatively recrystallizes in part with crystalline regions separated by amorphous material. Conversely, at very high compressions or tensions the resulting ion velocities are so high that the material falls apart and the simulation fails catastrophically. Consequently, although the procedure may succeed in realising an amorphous transition, only certain values for the compression are effective in generating a crystalline final structure. We have found that for rocksalt structured oxides the tolerances are quite broad. Conversely, for the fluorite structured CeO_2 the tolerance is narrow.[40]

It is tempting to suggest that the simulated recrystallization models real recrystallization processes. However, the amorphous starting configurations are of high energy and do not therefore reflect real systems. Moreover, temperature scaling must be performed during the simulation to prevent the rapid buildup of large amounts of excess kinetic energy as the system evolves from the highly strained initial configuration, via an amorphous transition, to a crystalline phase with defects and reduced strain. In addition, the time scales required to effect the recrystallization are much smaller (typically one nanosecond) compared to real crystallization. The simulation is therefore a technique to derive a range of low-energy configurations, which comprise various structural features observed in real systems and the evolution or dynamical recrystallization bears little physical significance.

D. Generation of nanoparticles

To generate models for MgO, CaO, and SrO nanoparticles supported on BaO(001), a simulated amorphization and recrystallization methodology, developed previously,[24] was employed. Specifically, a 25 088 atom MgO slab, exposing {100} planes at each of the six surfaces, 56×56 atoms in area and 8 atoms high was placed on top of a BaO(100) support (Fig. 1). The surface of the BaO(001), comprising the simulation cell and repeated periodically, was 84×84 atoms (231.6 Å in the [010] and [100] directions) resulting in a surface area of approximately 54 000 Å^2. The MgO slab was then expanded by 31% and dynamical simulation, performed

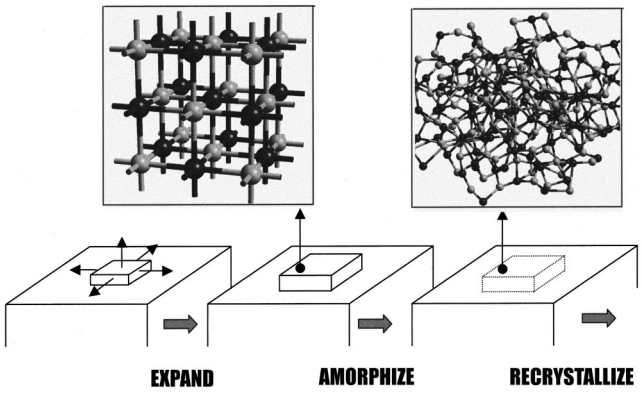

FIG. 1. Schematic illustrating the amorphization and recrystallization methodology as applied to the generation of supported nanoparticles. A slab of MgO is placed on a BaO(001) substrate and expanded linearly by 31%; a small segment of the BaO nanoparticle is depicted illustrating the rocksalt structure of the material. Upon the application of dynamical simulation, performed at high temperature, the considerable (tension induced) strain within the MgO lattice results in the amorphization of the nanoparticle. Again a small segment of the nanoparticle is presented to depict the amorphous transition. Upon prolonged dynamical simulation, the amorphous MgO recrystallizes.

at 2000 K for 5 ps, was applied, which resulted in the generation of a (tension induced) amorphous MgO ''slab'' on top of the BaO(001) substrate (Fig. 1). To recrystallize the slab, dynamical simulation was applied to the system for 855 ps at 2500 K, 5 ps at 1500, 1000, and 500 K, and 110 ps at 0 K.

To generate the SrO and CaO nanoparticles supported on a BaO(001) substrate, the system comprising an amorphous MgO slab supported on the BaO(001) was taken and all the magnesium ions switched for either strontium or calcium. These two systems were then recrystallized. In particular, dynamical simulation was performed on the CaO/BaO(001) system for 160 ps at 2000 K, 180 ps at 1500 K, 65 ps at 1000 K, 135 ps at 500 K, and finally 75 ps at 0 K. For the SrO/BaO(001) system, dynamical simulation was performed for 189 ps at 2500 K, 10 ps at 1500 K, 60 ps at 1000 K, 5 ps at 500 K, and finally 200 ps at 0 K.

It is apparent that the (amorphous) MgO/BaO will have a higher energy compared with the CaO/BaO and especially the SrO/BaO system. However, the simulation strategy is to generate simply an amorphous structure to facilitate high mobility of the ions such that they can then move to evolve a low-energy configuration. The recrystallization step, which leads to the final low-energy configuration is therefore more important compared with the initial amorphous structure. Essentially, the primary factor in controlling the recrystallization is the lattice misfit associated with the system and the interfacial interactions, which will be apparent when comparing the final structures for the three systems in the following section.

Preliminary test simulations on the amorphization and recrystallization strategy as applied to rocksalt structured oxides suggest that assuming the material undergoes an amorphous transition, the degree of compression or tension imposed to facilitate the amorphous structure has little effect on the final structures. Specifically, the tolerances for effective recrystallization (as alluded to above) are relatively broad.

To ensure recrystallization, the temperature is scaled homogeneously and stepped down. At each stage, the energies are allowed to equilibrate, which gives rise to the long simulation times. Any cooling rate in molecular dynamical simulation will be excessively quick due to the short real times accessible. We have, through ensuring equilibration at each stage performed simulations, which allow the system to recrystallize as efficiently as possible. The use of continuous cooling, although attractive, would remove our ability to monitor and control this process, as we could not establish easily if the cooling rate was too quick to allow the formation of low-energy structures or too slow so as to be inefficient. In our approach, we can check at each temperature step whether the system has equilibrated, which enables us to exact some control over the efficiency of the recrystallization.

III. RESULTS

To aid understanding and interpretation of the behavior of SrO, CaO, and MgO nanoparticles supported on BaO(001),

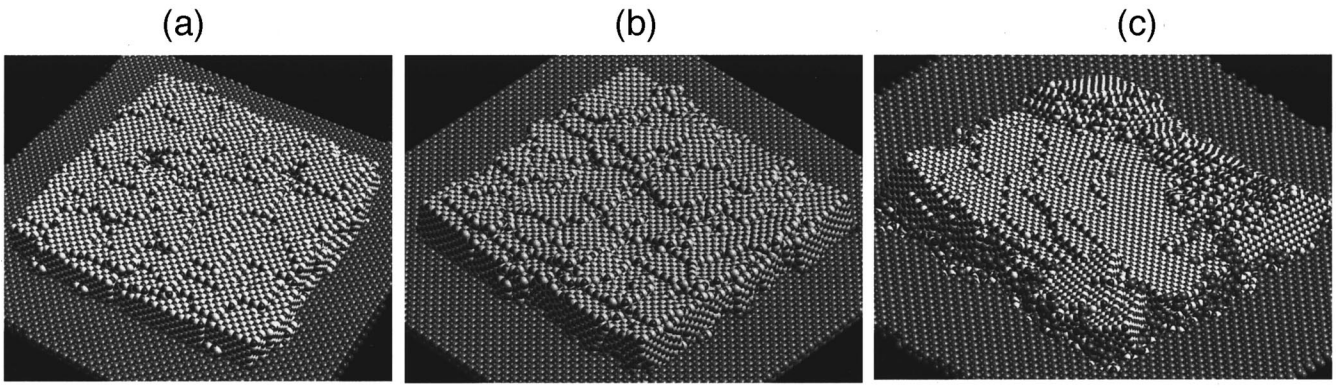

FIG. 2. Sphere model representations of the final atom positions comprising (a) the SrO, (b) CaO, and (c) MgO nanoparticles supported on a BaO(001) substrate. Oxygen ions are depicted by dark spheres, barium the lighter spheres, and Sr, Ca, or Mg the white spheres.

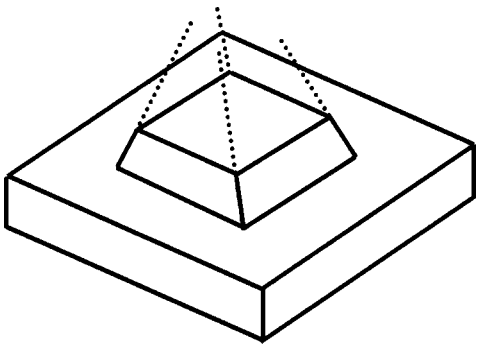

FIG. 3. Schematic illustrating the pseudopyramidal slab morphologies of the SrO and CaO nanoparticles when supported on BaO(001).

we consider the morphologies of the nanoparticles, the interfacial structures, the densities of ions as a function of distance from the interface, and also the radial distribution functions (RDF's).

A. Nanoparticle morphologies

To determine the morphologies of each nanoparticle, graphical techniques were employed to visualize and manipulate the atoms comprising the nanoparticles and underlying BaO substrate. The atom positions for the SrO, CaO, and MgO nanoparticles supported on BaO(001) are presented in Figs. 2(a)–2(c) respectively. The SrO and CaO nanoparticles demonstrate well defined cubic (slab) morphologies, $150\times150\times22$ Å (SrO) and $140\times140\times20$ Å (CaO) in size (the thickness is perhaps rather ambiguous owing to partial filling of the surface layers), with {100} surfaces exposed at each of the five faces of the crystal and presented also at the interfacial plane.

Inspection of the SrO and CaO (001) surfaces reveal the presence of a multitude of steps traversing the [100] and [010] directions. These steps are predominantly monatomic although a few diatomic steps are also present. In addition, the four sides of each nanoparticle are stepped and slope inwards by about 10° (CaO) and 5° (SrO) giving a similar morphological appearance to the base of a square pyramid; a schematic to aid interpretation is presented in Fig. 3. Analysis, using graphical techniques, revealed that within the central region of the CaO nanoparticle the (002) planes lie parallel with the underlying BaO(002) planes. Conversely, as one traverses to the edges of the nanoparticle the CaO(002) planes bend upwards ([001]) by as much as 0.5 Å resulting in the (002) planes having what can perhaps be described as a ''concave lens'' shaped structure. Towards the outermost regions of the nanoparticle, the CaO(002) planes lie vicinal with respect to the substrate, which gives rise to the sloping sides of the nanoparticle. Similar, albeit less marked, behavior can be observed for the SrO/BaO(001) system.

Remarkably, the MgO/BaO nanoparticle is significantly more complex and comprises a central plateau region [vicinal MgO(001)/BaO(001)], with intersecting crystallites at each of the four corners. These crystallites can be categorized loosely as having triangular pyramidal morphologies; inspection of the crystallite [far right of Fig. 2(c)] reveals

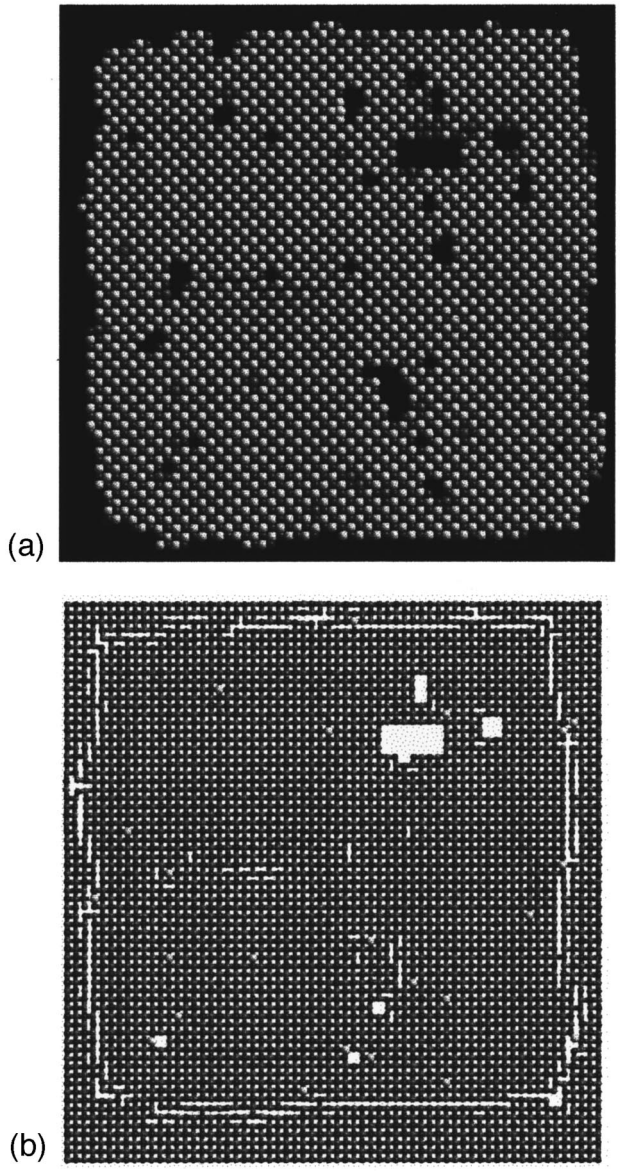

FIG. 4. Sphere model representations depicting the atom positions of (a) the interfacial SrO(002) plane of the nanoparticle and (b) the interfacial BaO(002) plane of the substrate. Oxygen ions are depicted by the dark spheres, barium the lighter spheres, and strontium, the white spheres.

vicinal MgO(111)/BaO(001). The central MgO region is rotated by about 6° about an axis perpendicular to the interfacial plane. The intersection of these crystallites at the corner with the central plateau region results in the formation of an array of grain boundaries. However, owing to the complexity of the structure, including curvature of the (002) planes, it was not possible to characterize the orientational relationships between these boundaries. Screw-edge dislocations were also identified to have evolved within the central plateau region of the MgO slab. In addition, barium ions from the substrate are observed to decorate the outer surfaces of the MgO nanoparticle. Further details of this system have been published elsewhere.[22]

A simulation study of Huang and Bartell on the structure of potassium iodide nanoparticles suggests that the solid

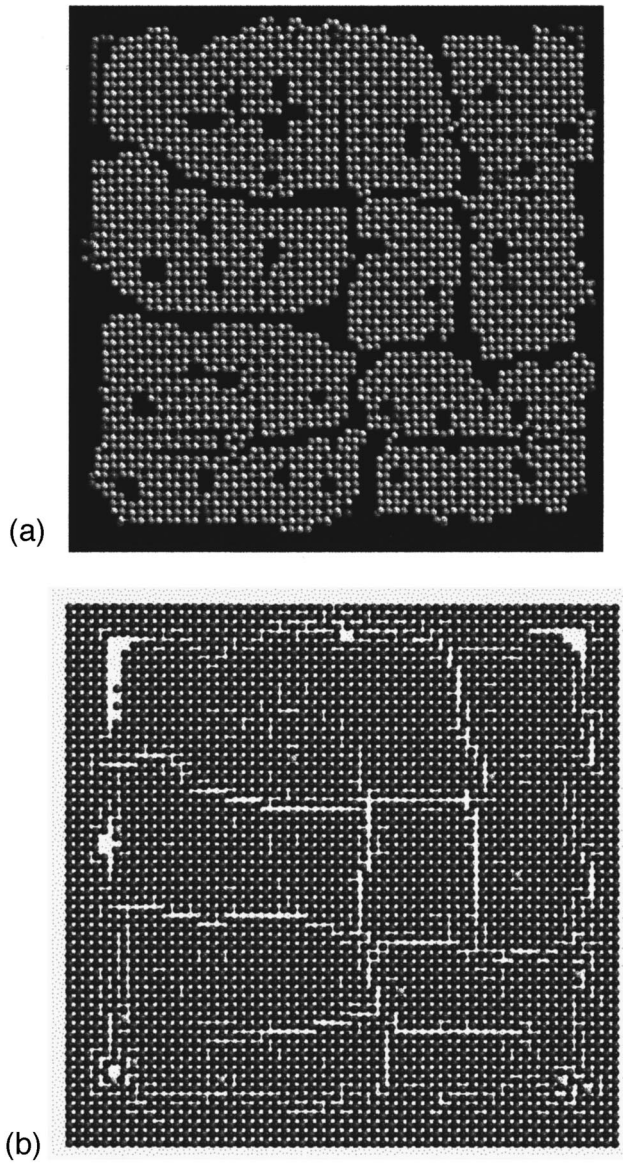

FIG. 5. Sphere model representations depicting the atom positions of (a) the interfacial CaO(002) plane of the nanoparticle, (b) the interfacial BaO(002) plane of the substrate. Oxygen ions are depicted by the dark spheres, barium the lighter spheres, and calcium, the white spheres.

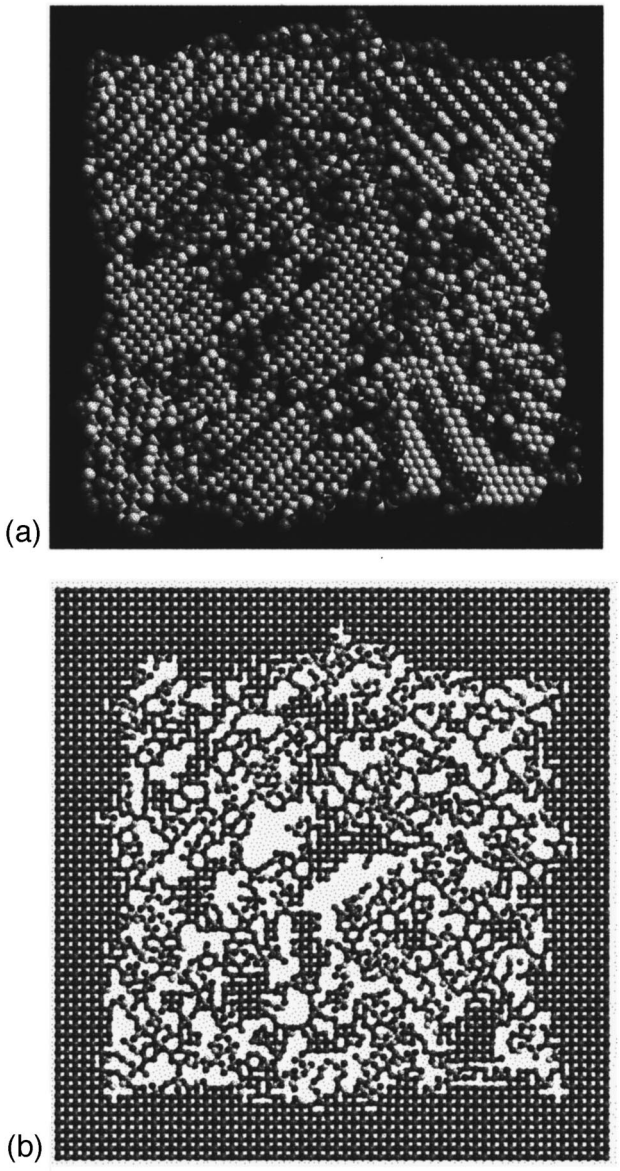

FIG. 6. Sphere model representations depicting the atom positions of (a) the interfacial MgO (''*hkl*'') plane of the nanoparticle, (b) the interfacial BaO(002) plane of the substrate. Oxygen ions are depicted by the dark spheres, barium the lighter spheres, and magnesium, the white spheres.

nanoparticles accommodate the rocksalt structure and are well faceted exposing (001) surfaces.[41] Monodisperse crystalline nanoparticles of barium titanate, with diameters ranging from 6–12 nm, have been synthesized showing cubic morphologies.[17] Wollschlager *et al.* demonstrated that MgO, when deposited on Mg thin films form ordered MgO grains with different rotational orientations.[42]

B. Interfacial regions

The interfacial SrO, CaO, and MgO layers are shown in Figs. 4(a), 5(a), and 6(a) with their respective BaO interfacial layers shown in Figs. 4(b), 5(b), and 6(b). Interfacial distances between the nanoparticle and the underlying BaO substrate are calculated to be 2.60, 2.40, and 2.05 Å for the SrO, CaO, and MgO nanoparticles, respectively, compared with {002} distances of 2.58 (SrO), 2.40 (CaO), and 2.10 Å (MgO) within the parent oxides.

1. SrO/BaO(001)

The interfacial SrO and BaO(002) planes are depicted in Figs. 4(a) and 4(b), respectively. The SrO lies coherent with respect to the underlying support with cations and anions lying directly above their respective counterions of the underlying support. The interfacial SrO plane comprises many isolated strontium and oxygen vacancies, associated defect vacancies (2–6 vacant sites) and larger vacancy associations,

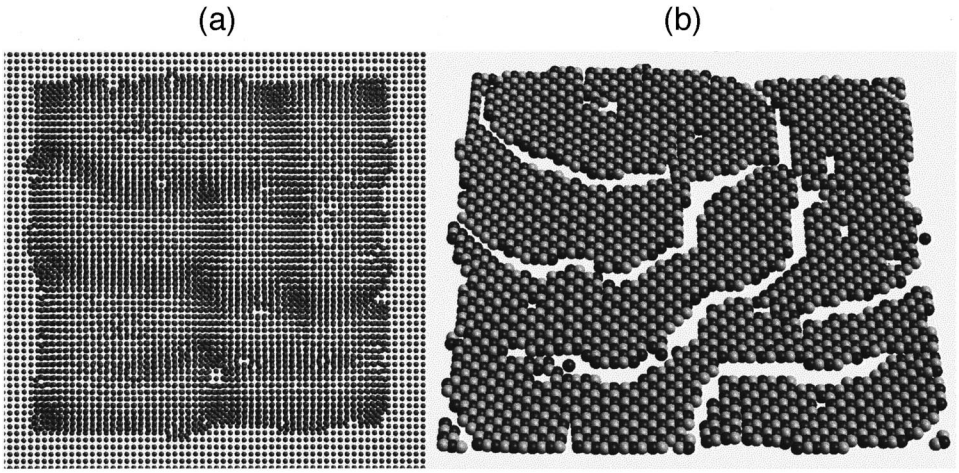

FIG. 7. Sphere model representations depicting the atom positions of (a) the interfacial CaO(002) and BaO(002) planes, (b) perspective view of the CaO overlayer. The ''light'' regions in (a) are where the ions maintain coherence across the interfacial plane and darker regions are where the ions fall out of alignment.

which can perhaps be classed as ''voids.'' In addition, isolated and associated barium substitutionals can be seen, which occupy displaced strontium lattice positions. A similar defective structure is also exhibited by the underlying interfacial BaO plane. An additional feature of this system is that at the edges of where the SrO nanoparticle sits on the surface of the BaO substrate, the interfacial BaO plane exhibits cracks or fissures with Ba-O distances ranging from about 2.5 to 3.5 Å. This indicates that the BaO beneath the SrO has contracted slightly to accommodate a coherent interfacial structure.

2. CaO/BaO(001)

For this system, the contraction of the underlying interfacial BaO plane is much more pronounced [Fig. 5(b)] with cracks and fissures clearly evident; Ba-O distances within such cracks range from about 2.5 to 3.8 Å. Moreover, the contraction is limited not only to the perimeter described by the overlying CaO nanoparticle, as is apparent for the SrO/BaO system, but are also clearly *evident* within the interfacial area covered by the overlying CaO nanoparticle. Clearly, in the case of a CaO nanoparticle the strain within the BaO is much greater and required cracks to form at closer intervals in an attempt to maintain a coherent structure.

Inspection of the interfacial region of the overlying CaO nanoparticle, Fig. 5(a), suggests clusters of CaO, which interface the main body of the CaO nanoparticle with the underlying BaO substrate. Directly underlying these CaO clusters, the BaO contracts, to maximize interfacial interactions. That clusters evolve at the interfacial region, as opposed to complete filling of the interfacial CaO(002) plane, indicates that there is a reduced density of ions. Such an observation is supported by previous theoretical studies.[23,43]

Similar to the SrO/BaO(001) system, the interfacial BaO(002) plane comprises isolated calcium ions, which have migrated from the CaO slab to occupy barium lattice sites. The barium ions displaced occupy calcium lattice sites within the interfacial CaO(002) plane of the overlying nanoparticle. In addition, many isolated and associated vacancies are present within the interfacial CaO(002) plane. It is interesting to note that the top left corner of the CaO nanoparticle [Fig. 5(a)] comprises six BaO species, which have migrated from the interfacial BaO(002) plane. Similarly, three BaO species have migrated to the top left corner of the CaO slab.

A plan view of the interfacial CaO and BaO planes are shown in Fig. 7(a). The figure shows various regions where the cations and anions of the CaO are perfectly aligned (coherent) with their respective counter ions of the underlying

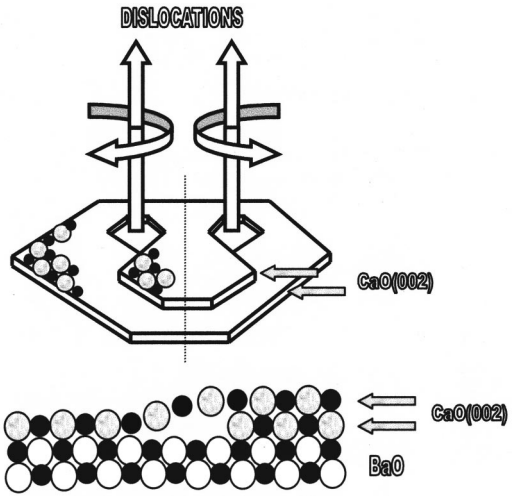

FIG. 8. (Bottom) 2D schematic illustrating interfacial CaO ions lying coherent with respect to the underlying BaO and as one traverses to the right of the figure one can observe the ions move (via a dislocation) out of alignment. Notice that as the ions move out of alignment, owing to the presence of the dislocation, the distances between ions increases reducing the deleterious influence of isovalent ions in close proximity. Far right, the ions again become coherent. An additional schematic (top) illustrates the location of screw-edge dislocations, which facilitate this coherence misalignment transition. The dotted line shows where the bottom figure lies with respect to the top.

BaO support. These regions of registry coincide with the central region of the clusters seen in Fig. 5(a). Towards the edges of each cluster (and at the perimeter of the whole nanoparticle), the ions move out of alignment.

In Fig. 7(b), a perspective view of the interfacial CaO(002) plane is shown. The ''gaps'' in the figure relate to parts of the CaO lattice, which bend up (tilt), via screw-edge dislocations (no dislocations were observed in the SrO nanoparticle), to form a second plane over the first (a schematic to aid interpretation is presented in Fig. 8). If one then compares Fig. 7(a) with Fig. 7(b) it can be adjudged that regions of misalignment coincide with where the CaO starts to overlay the interfacial CaO plane. Screw-edge dislocations reside in such regions of misalignment. Graphical techniques were employed to locate and then deconvolute, with respect to the adjoining lattice, the structures of the dislocations; the core structure of one particular screw-edge dislocation is depicted in Fig. 9.

An experimental study by Ernst *et al.* on the $SrZrO_3/SrTiO_3$ system, fabricated using metal-organic deposition of $SrZrO_3$ layers on $SrTiO_3(001)$ single-crystal substrates and imaged using high-resolution transmission electron microscopy (HRTEM), revealed that the lattice misfit is accommodated, in part, via the evolution of dislocations.[44] Moreover, such dislocations reside in regions of lattice misalignment in accord with the findings of this present study. In addition, a study by Jia *et al.* on $BaTiO_3$ thin films deposited by laser ablation on MgO(001) substrates observed (using HRTEM) that the lattice misfit associated with the system was accommodated via the evolution of dislocations within the thin film.[10] Wollschlager *et al.* who employed spot profile analysis of low-energy electron diffraction to investigate the surface morphology of MgO films grown on Ag(001) suggest that the strain associated with the system (mismatch +3.4%) leads to buckling of the MgO thin film and dislocations evolve. Moreover, the authors suggest that there are no antiphase boundaries, which helps facilitate strain relief without incurring electrostatic repulsion; a schematic, analogous to the model proposed by Wollschlager *et al.*, is presented in Fig. 8. In addition, in this present study we suggest the evolution of dislocations with *mixed* screw-edge character.

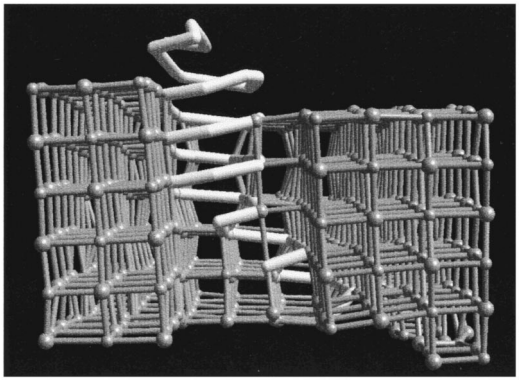

FIG. 9. Ball and stick representation of the ion positions of a small segment of the CaO nanoparticle, which includes a screw-edge dislocation. The core structure of the dislocation (light) is shown within part of the surrounding CaO lattice of the nanoparticle. Ions have been removed to ensure visibility of the dislocation core.

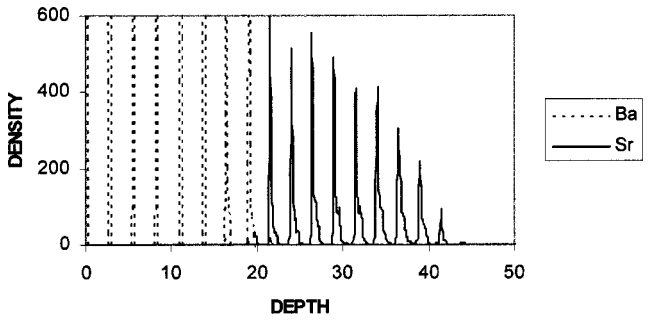

FIG. 10. Strontium and barium ion densities, calculated as a function of distance (measure in Å) along the [001] of the SrO/BaO(001) system. The ionic densities were integrated over a thickness of 0.1 Å.

3. MgO/BaO(001)

Here, the interfacial regions are so complex that it becomes almost intractable to rationalize the structure. Accordingly, only a few salient details are given. The interfacial BaO plane is highly defective comprising many voids and BaO and MgO clusters. Indeed, magnesium ions comprise 30% of the total cations within the interfacial BaO(002) plane. For the interfacial MgO region, the MgO is seen to expose various (ill defined) orientations with respect to the underlying BaO. However, we suggest tentatively, two orientations, which are perhaps evident. The first is vicinal MgO(001)/BaO(001) [center and left of Fig. 6(a)] and vicinal MgO(111)/BaO(001) (bottom right corner). The latter is deduced from observing the exposure of small regions of pure magnesium or oxygen planes in a hexagonal arrangement. It is also interesting to note that barium ions, which have migrated from the interfacial BaO plane occupy (grain boundary) positions between the various crystallites comprising the MgO nanoparticle. There are no observable regions of coherence between the MgO and underlying BaO substrate.

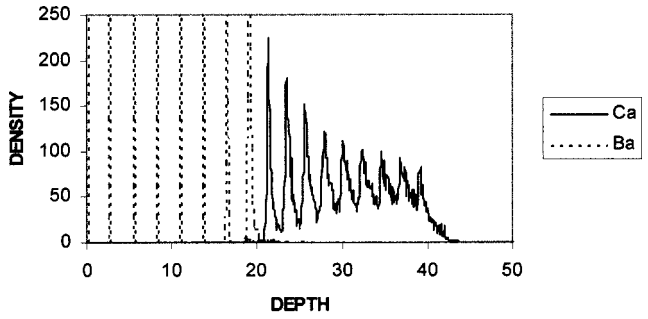

FIG. 11. Calcium and barium ion densities, calculated as a function of distance (measure in Å) along the [001] of the CaO/BaO(001) system. The ionic densities were integrated over a thickness of 0.1 Å.

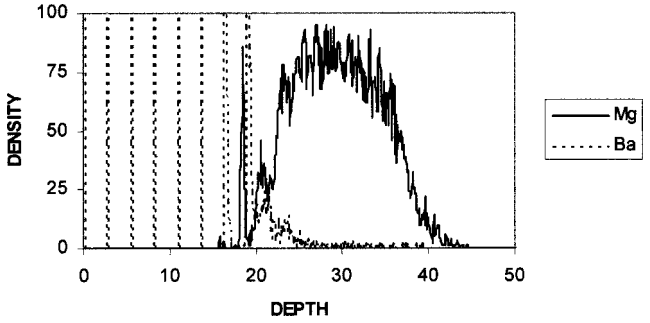

FIG. 12. Magnesium and barium ion densities, calculated as a function of distance (measure in Å) along the [001] of the MgO/BaO(001) system. The ionic densities were integrated over a thickness of 0.1 Å.

C. Ion densities

To aid structural interpretation of the nanoparticles, the ion densities, as a function of distance normal to the interfacial plane, are presented for the SrO/BaO, CaO/BaO, and MgO/BaO systems in Figs. 10–12, respectively. The ion densities have been calculated using the MDPREP code[45] to indicate any changes in the layers of the rocksalt structured lattices. The ion density $z(x)$ is defined as the number of atoms of a given type, within a range of perpendicular positions in the simulation cell and normalized to the average density

$$z(x)=\frac{V}{N}\frac{1}{A\delta x}\left\langle \sum_i \delta(x-x_i)\right\rangle, \tag{2}$$

where V is the simulation cell volume, N is the number of atoms of the given type, A is the area of the interface, x_i is the perpendicular height of atom i and δx is the histogram width over which the δ function gives one. A value of 1.0 thus represents the average density for that species within the entire simulation cell (including the vacuum) with larger values indicating increased density and the formation of well-defined crystal planes.

1. SrO/BaO(001)

In Fig. 10, the ion densities of both the SrO and BaO are presented. The bottom of the BaO substrate is located at a depth of zero with the first eight peaks corresponding to BaO(002) planes. The first six peaks relate to barium ions, which are within region II, while the following two are within region I. Since ions within region II are kept fixed during the simulation, the first six peaks are sharp. Conversely, barium ions within region I are allowed to move. Accordingly, the remaining two peaks, which correspond to barium ions within region I are broadened, reflecting ionic relaxation in this interfacial region as the BaO substrate responds to the overlying nanoparticle.

The remaining peaks within the figure relate to the overlying SrO nanoparticle, which one can estimate as about 22 Å thick [the distance from the interfacial BaO(002) peak to the outermost SrO(002) peak]; the value is approximate owing to partial filling of the outermost SrO planes. In addition, the nanoparticle comprises around 8–9 (002) layers with partial occupancy of the uppermost (001) surface as indicated by the small outer peaks. Figure 2(a) shows graphically the incomplete filling of the surface layer, which comprises many steps and ledges.

We also notice peak broadening (to the right) corresponding to the SrO nanoparticle, which can be attributed to the slight bending of the SrO(002) planes from the center to the edges of the nanoparticle as alluded to in the previous section. SrO(002) interplanar distances, estimated from Fig. 10, are calculated to be 2.45 or 0.12 Å lower than the parent oxide with an interfacial SrO/BaO separation of 2.59 Å. Surprisingly, the calculations indicate that the BaO(002) interplanar separation is reduced from 2.73 Å (parent oxide) to 2.55 Å for the two interfacial BaO(002) planes.

2. CaO/BaO(001)

For the CaO/BaO(001) system (Fig. 11) a similar trace to that of the SrO/BaO(001) system is evident. The two peaks corresponding to the interfacial BaO(002) planes are broadened further compared with the SrO/BaO(001) system reflecting the increased interfacial relaxation of the BaO substrate in response to the CaO nanoparticle. The nanoparticle is estimated to be about 20 Å thick and comprises 8–9 CaO(002) layers, again exhibiting partial occupancy of ions at the outermost surface. The peaks, corresponding to the CaO(002) planes, are much broader compared with the previous SrO/BaO(001) system with the density failing to fall to zero between the peaks owing to the considerable curvature of the CaO(002) planes. This is a consequence of the ions at the outermost regions of the nanoparticle having moved more than a (002) lattice spacing such that the density at a particular distance includes ions from two different CaO(002) planes.

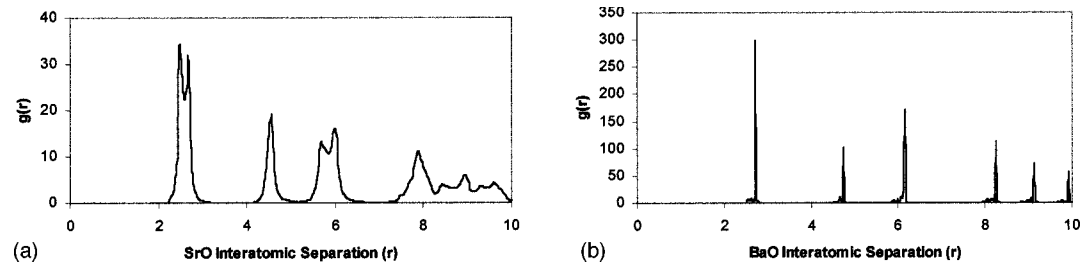

FIG. 13. Calculated (a) SrO RDF, (b) BaO RDF for the SrO nanoparticle supported on a BaO(001) substrate. Interatomic separations are shown in Å.

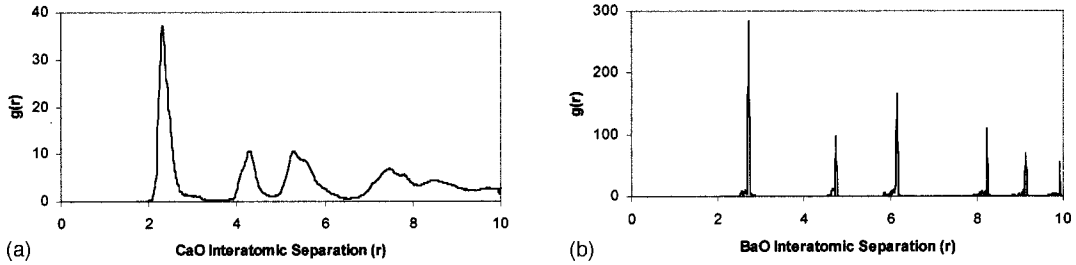

FIG. 14. Calculated (a) CaO RDF, (b) BaO RDF for the CaO nanoparticle supported on a BaO(001) substrate. Interatomic separations are shown in Å.

The figure indicates also a small amount of intermixing of barium and calcium ions across the interfacial plane with barium ions extending as far as 8 Å into the CaO lattice. Interplanar CaO(002) distances are calculated to be about 2.2 Å, which is 0.2 Å smaller than interplanar distances in the parent oxide; the interfacial distance is calculated to be 2.4 Å. In addition, the two interfacial BaO(002) lattice spacings are reduced by 0.2 Å compared with the parent material.

3. MgO/BaO(001)

Figure 12 depicts the density of ions, as a function of distance normal to the interfacial plane, for the MgO/BaO(001) system. The trace, while exhibiting characteristically sharp peaks for the underlying BaO substrate, is markedly different to the traces for the previous two systems. The two interfacial BaO planes are much broader indicating considerable relaxation of ions within this region. Barium ions can also be seen to migrate into the MgO nanoparticle as far as the surface of the MgO nanoparticle [as can be observed in Fig. 2(c)]. In addition, there are no peaks, which could be attributed to MgO(002) planes within the figure. This is because the trace includes integrations of the ionic density from all the various misoriented crystallites and peaks corresponding to MgO(002) planes are not resolved.

The observation of diffusion of ions into the nanoparticles is supported by the molecular beam epitaxy study of the growth of Fe_3O_4/NiO thin films by Lind *et al.*[46] They showed that interfacial diffusion of the Fe_3O_4 and NiO layers occurs of the order of one or two atomic layers. This is the order of diffusion that we see within the lower misfit systems, which are closer to the experimental systems of Lind *et al.*

D. Radial distribution functions

Radial distribution functions (RDF's) were used to investigate the structural disorder of the thin films and were calculated using the MDPREP code.[45] The RDF is defined as the probability of finding an atom at a distance r from another atom compared to a homogeneous distribution[47] and is given by

$$g(r)=\frac{V}{N_1N_2}\frac{1}{4\pi r^2\delta r}\left\langle \sum_i \sum_{j>i} \delta(r-r_{ij})\right\rangle, \qquad (3)$$

where V is the volume, N_1 and N_2 are the atom types of the RDF. The delta function must give rise to a value of one for a range of r (δr), allowing the formation of a fine grain histogram. The RDF thus tends to 1.0 at long distances with sharp peaks indicating a regular lattice structure. For amorphous or liquid systems the RDF shows characteristically a small number of broad peaks at short distance, indicating short range order, superimposed on an oscillating trace to 1.0, which indicates the loss of long range order.[47] For the systems considered in this present study, normalization is performed by using a homogeneous distribution for the whole simulation cell, which contains significant regions of empty space. The RDF is likely therefore to be larger than 1.0 at short distances and only tend to 1.0 at very long distances when multiple simulations cells have been considered.

1. SrO/BaO(001)

SrO and BaO RDF's for the SrO/BaO(001) system are presented in Figs. 13(a) and 13(b), respectively. The figures indicate that both the SrO nanoparticle and underlying BaO substrate maintain a rocksalt type structure. For the BaO substrate the RDF is sharp indicating little perturbation of the interfacial ions in response to the overlying SrO nanoparticle. Nearest neighbor Ba-O distances are calculated to be 2.73 Å, which are commensurate with the parent oxide. Additional nearest neighbor peaks at 2.57, 2.63, and 2.78 Å are also evident from the RDF. For the overlying SrO nanoparticle, the peaks are broad and split, with nearest neighbor

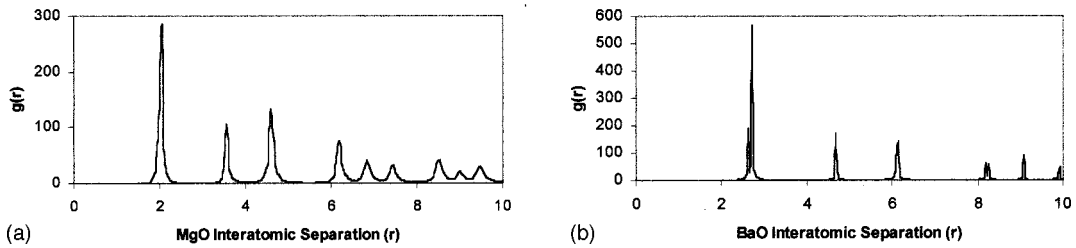

FIG. 15. Calculated (a) MgO RDF, (b) BaO RDF for the CaO nanoparticle supported on a BaO(001) substrate. Interatomic separations are shown in Å.

Sr-O distances of 2.5 and 2.7 Å (range 2.3 to 2.8 Å). One can (loosely) assign the 2.7 Å peak as corresponding to the expansion of the SrO in the interfacial plane ([100] and [010]) to ensure coherence with the underlying BaO substrate with the peak at 2.5 Å reflecting the (contracted) SrO(002) interplanar distances. Average nearest-neighbor Sr-O distances calculated *within* each SrO(002) plane (RDF not shown) are 2.72 Å (interfacial plane), 2.70, 2.69, 2.68, 2.67, 2.67, 2.55, and 2.55 Å (surface plane) indicating a slight contraction in the SrO lattice as one traverses from the interfacial plane to the surface of the SrO nanoparticle.

2. CaO/BaO(001)

The calculated CaO and BaO RDF's for the CaO/BaO(001) system are presented in Figs. 14(a) and 14(b), respectively. The RDF for the BaO support is sharp, with nearest-neighbor Ba-O distances of 2.73 Å. The RDF's for the overlying CaO is broad with nearest-neighbor Ca-O distances of 2.3 Å (range 2.1 to 3.5 Å); a shoulder at 2.5 Å is also evident. Average nearest-neighbor Ca-O distances for ions within each CaO(002) plane (RDF not shown) are calculated to be about 2.4 Å (range 2.2 to 3.2 Å) or commensurate with the parent oxide and 0.33 Å smaller than the underlying BaO substrate. This suggests that the CaO does not lie commensurate with the BaO support. However, this is an average distance and from Fig. 7(a) one can observe regions where the CaO appears to lie coherent with respect to the BaO and adjoining regions where the cations and anions across the interfacial region are misaligned. We suggest that in regions of coherence, the CaO is under tensile stress to enable accord with the lattice parameter of the underlying BaO. Conversely, in regions of misalignment the CaO is compressed. And while this is true in general within regions of coherence and misalignment, inspection of the actual bond distances in these regions exhibit considerable variability as indicated by the range (2.2 to 3.2 Å) of CaO distances within the CaO(002) planes.

3. MgO/BaO(001)

The calculated SrO and BaO RDF for the MgO/BaO(001) system are shown in Figs. 15(a) and 15(b), respectively. The BaO RDF exhibit sharp split peaks. Nearest-neighbor Ba-O distances are calculated as 2.62 and 2.73 Å with minor peaks at 2.58 and 2.78 Å. Conversely, the peaks within the RDF for the overlying MgO nanoparticle are sharper compared with either the supported CaO or SrO nanoparticles. Average nearest-neighbor Mg-O distances are calculated to be 2.05 Å (range 1.9 to 2.2 Å).

IV. DISCUSSION

The various morphological, epitaxial, and structural features for each of the three systems are summarized in Table I. We attempt now to rationalize the structures in terms of the misfits associated with each system.

A. SrO/BaO(001)

For the SrO/BaO(001) the lattice misfit is, at −7%, relatively small. Consequently, ions comprising the SrO nanoparticle are able to maintain registry with the underlying counter ions of the BaO substrate and a nanoparticle that is coherent with respect to the substrate evolves. Clearly, for a nanoparticle 8–9 (002) layers thick, the energy required to tension the SrO lattice by 7% and into coherence with respect to the underlying BaO is more than compensated for by the favorable interactions between counter ions. In addition, we suggest that the underlying BaO contracts slightly, resulting in the formation of fissures or cracks within the interfacial BaO(002) plane [Fig. 4(b)] to help ensure coherence, thereby maximizing the interactions across the interfacial region.

We also advocate that the defects present at the interfacial region will help reduce (locally) the lattice misfit further stabilizing the system. For example, owing to the larger size of the barium ions compared with strontium, the barium ions migrating from the support into the SrO nanoparticle at the interfacial region will result in an expansion of the SrO, reducing locally the lattice misfit. Similarly, the migration of the strontium ions displaced into the BaO support will contract the underlying BaO interfacial plane. In addition, the evolution of vacancy clusters or voids will facilitate increased ionic relaxation, which may help maximize favorable interactions between counter ions.

Visualization shows that the sides of the nanoparticle are tilted, resulting in a pseudopyramidal morphological appearance. This helps facilitate a reduction of the lattice parameter as one traverses from the interfacial plane to the surface of the SrO nanoparticle. The driving force for such behavior is the reduction in strain energy within the SrO. Specifically, as one proceeds from the interfacial plane, where the SrO is constrained under tension to ensure coherence with the underlying BaO, to the surface of the SrO, the lattice parameter gradually reduces to be more in accord with the parent oxide. Consequently, the strain energy terms are reduced.

One perhaps surprising observation is that the interplanar SrO(002) separation is 0.12 Å smaller than in the parent oxide. Conversely, within the plane the interionic distances are about 0.12 Å greater (to enable coherence). The strain in the lattice and subsequent anisotropic structure will have implications for the chemical and physical properties of the nanoparticle.

B. CaO/BaO(001)

For the CaO/BaO system, which is associated with a −15% lattice misfit, the nanoparticle does not maintain coherence across the full interfacial area. Clearly, the energy required to strain the CaO into coherence with respect to the underlying BaO substrate is higher than the energy returned by having counter ions in close proximity. Consequently, the simulations advocate that only certain regions (around 200–300 $Å^2$) of the CaO maintain coherence with respect to the underlying BaO; the surrounding regions fall out of alignment. Within regions of misalignment, isovalent ions are in close proximity destabilizing the system. However, such unfavorable interactions are reduced via the evolution of screw-edge dislocations, which act to preserve low interfacial distances for coherent CaO/BaO regions, while maximizing

TABLE I. Summary of the MO (M = Sr,Ca,Mg) nanoparticles supported on BaO(001) giving the lattice parameters for the MO and misfit (F) of each system; the morphological features and size of the nanoparticles including MO distances within each MO(002) plane and distances between MO(002) planes; epitaxial relationships identified; features pertaining to the interfacial regions and interfacial separations and defects identified within the supported nanoparticle and underlying BaO substrate.

Nano-particle	F	Morphology	Epitaxy	Interfacial region	Defects
SrO	5.16 Å	150×150×22 Å slab	SrO(001)/BaO(001)	Slight perturbation of interfacial BaO(002) at perimeter of nanoparticle	No dislocations
	−7%	Pyramidal sloping (5°) sides	Fully coherent		Isolated vacancies
		Monatomic (few diatomic) steps on nanoparticle surface	Broad SrO RDF (lattice strain)	Interfacial distance: 2.60 Å	Vacancy clusters and voids
					Sr, Ba substitutionals
		Sr-O distances 2.69; 2.45 Å			Migration of Ba into nanoparticle (1–2 planes)
CaO	4.80 Å	140×140×20 Å slab	CaO(001)/BaO(001)	Cracks/fissures in BaO surrounding coherent regions of overlying CaO	Screw-edge dislocations Isolated vacancies
	−15%	Pyramidal sloping (10°) sides	Vicinal CaO(001)/BaO(001)		Vacancy clusters
		Significant plane bending	Coherent domains (200–300 Å^2) separated by misaligned regions	Reduced ionic density	Ca, Ba substitutionals
		Monatomic (few diatomic) steps on nanoparticle surface	Broad CaO RDF (lattice strain)	Interfacial distance: 2.40 Å	Migration of Ba into nanoparticle (1–2 planes)
		Ca-O distances 2.40; 2.20 Å			
MgO	4.20 Å	approximate 125×125×20(25) ''slab''	Vicinal MgO(001)/BaO(001)	Considerable perturbation and mixing of interfacial planes	Grain boundaries
	−31%	Misoriented grains	Vicinal MgO(111)/BaO(001)	MgO and CaO clusters	Screw edge dislocations
		Significant plane bending	MgO(hkl)/BaO(001)		Considerable migration of Ba into nanoparticle
				Reduced ionic density	
		''Pyramidal'' morphology at corners	Misaligned grains	Interfacial distance around 2.05 Å	Ba ions decorate nanoparticle surface
			Sharp MgO RDF		
			No apparent coherency		

interfacial distances for the adjoining misaligned regions within the same CaO plane. For example, within misaligned regions, the distance between isovalent ions across the interfacial region is increased via screw-edge dislocations, which enable the CaO lattice to spiral up half a lattice parameter away from the underlying substrate. Such a phenomenon has been observed previously in simulations of CaO/MgO thin films.[23] In contrast, for the SrO/BaO(001) system, the critical thickness[48] for the nanoparticle has not been reached (owing to the smaller lattice misfit associated with the system) and therefore no dislocations were observed to have evolved in the lattice.

It is pertinent to propose that if the CaO/BaO nanoparticle were smaller (lower interfacial area), the nanoparticle would be able to maintain coherence and no dislocations would evolve, i.e., if the surface area of the nanoparticle in contact with the substrate were commensurate with the area of CaO maintaining coherence. It also follows that for a system with a smaller misfit, compared with the CaO/BaO system, such regions of coherence would be larger [as is observed with the SrO/BaO(001) system]. It is well documented[48] that dislocations within thin films evolve at a particular ''critical thickness,'' which is related to the associated lattice misfit and also (albeit less marked) preparative conditions. One might suggest therefore that (for a certain nanoparticle thickness) there is also a ''critical area'' for dislocation evolution associated with a particular system. Specifically, we propose that the size (surface area) of a nanoparticle will be related to its critical thickness to dislocation evolution although further studies will be necessary to explore this assumption. Since the presence of dislocations can influence considerably, the physical and chemical properties of a material, the phenomena of ''critical areas'' will be important with respect to the fabrication of new materials, which involve supported nanoparticles or strips such as electronic devices. Similar to the SrO/BaO(001) system, the CaO/BaO(001) system exhibits defect (substitutionals, vacancies/voids) which help facilitate locally a reduction in the lattice misfit.

Experimentally, James and Hibma observed that NiO, when deposited on MgO(001), lies coherent with respect to the substrate. Moreover, a critical thickness of 600 Å was attained after which dislocations evolve to relieve the strain within the lattice.[49] A simulation study by Ashkenazy *et al.* suggests that small Pt nanoparticles, supported on Pt will align themselves with the substrate. However, as the particle size increases, an array of grain-boundary dislocations evolve,[50] which, in part, supports the idea of a critical area associated with supported nanoparticles.

C. MgO/BaO(001)

For the MgO/BaO(001) system the lattice misfit is so high (−31%) that no areas of the MgO with respect to the underlying substrate were observed to lie coherent; rather the nanoparticle exists as various interconnecting crystallites with various misaligned and ill defined (difficult to resolve) orientations. It is interesting to note that while the RDF for the SrO and CaO nanoparticles were broad, the RDF for the MgO nanoparticle was, in comparison, relatively sharp with nearest-neighbor Mg-O distances in accord with the parent oxide. The data indicates that while the SrO and CaO nanoparticles are highly strained, there is comparatively less strain within the MgO nanoparticle. We suggest that owing to the high associated lattice misfit of the MgO/BaO system, there is no possibility of coherency and hence strain to bring the lattices into coherence. Moreover, in previous studies,[24] which explored the structures of completely covered thin film, the RDF for the thin film were sharp indicating considerably less strain within the thin film compared with the nanoparticles considered here (we note, however, that there is no data on SrO or CaO on BaO or systems with an associated negative lattice misfit). It is likely that the considerable strain within the nanoparticles may give rise to modification of their electronic properties.

One might propose that the interfacial BaO(100) plane is too defective and arises because of the considerable energy introduced into the system in order to generate an amorphous structure. However, we suggest that this is not the case. Inspection of the system after amorphization reveals the interfacial BaO(100) layer to be free of defects. It is only during recrystallization that the defects evolve within the system. We propose that the considerable perturbation and defective nature of the interfacial BaO(100) plane is a consequence of the high lattice misfit associated with this system. Specifically, the results indicate that as the lattice misfit associated with the system increases, so the interfacial layer of the substrate becomes more defective.

An important feature of the simulated amorphization and recrystallization strategy we have employed in this study is that it is capable of generating model structures, which are independent of the preparatory configurations. However, since the final structures appear similar to the starting structures, it is pertinent to question this assumption. This is important since if the final structures reflect, in part, the preparatory configuration, any artificial features within this starting structure may also appear within the final structures. We argue that this is not the case with our methodology. In particular, the nanoparticle is forced to go amorphous thereby eliminating any long-range structural features within the nanoparticle. For the final structure to reflect the initial structure, memory of the preparatory configuration must be retained somehow within the short-range structure of the amorphous solid, which is unlikely. Conversely, although there is no identifiable structure within the long range as identified by RDF, and visualization, there might conceivably be some ''pattern'' in the long range that we cannot resolve. Clearly, this philosophical suggestion is at present beyond the scope of investigation using the methods we have available. Rather we suggest that the final structure appears similar to the preparatory configuration owing to the fact that the oxide prefers to expose {001} facets since they are the most stable, which gives rise to the characteristic slab morphological appearance of the nanoparticles. Indeed, experimentally, it is found that MgO exposes predominantly the (001) face when supported on Si(111) and glass.[51] In addition, previous work on the MgO/SrO(011) system, revealed that the supported MgO transformed from exposing the MgO(011) surface at the interface and surface of the film

(preparatory configuration) to exposing the (more energetically stable) (001) at both surfaces via the amorphous transition.[34] This provides further support to suggest that the amorphization and recrystallization strategy can eliminate features associated with the preparatory configuration. Moreover, for the MgO/BaO(001) system considered in this present study, the various rotations, and orientations of the various crystallites comprising the MgO nanoparticle are markedly different from the preparatory configuration [Fig. 2(c)].

One might perhaps expect the oxide nanoparticle to adopt a ''droplet'' appearance. Indeed, we have observed this convex lens-type morphological appearance for SrO nanoparticles supported on MgO(001) and have rationalized its formation based upon the high positive lattice misfit associated with this system.[52] Conversely, for the systems considered in this present study, which are all associated with negative lattice misfits, the [002] planes comprising the nanoparticle exhibit curvature in the opposite sense (concave lens-type morphology) to a droplet.

V. CONCLUSIONS

We have shown that employing a simulated tension induced amorphization and recrystallization methodology, models for metal oxide nanoparticles supported on an oxide substrate can be generated. For oxide nanoparticles supported on an oxide substrate with ''low'' [−7%; SrO/BaO(001)] associated lattice misfits, the nanoparticle lies coherent with respect to the underlying substrate. However, as the lattice misfit increases [−15%; CaO/BaO(001)], the strain energy becomes prohibitive for the nanoparticle to maintain coherence with the substrate and regions where the lattices fall out of alignment become interdispersed with regions of coherence. The misaligned regions comprise screw-edge dislocations, which enable the lattice to spiral away from the substrate reducing energetically deleterious interactions between isovalent ions. We suggest that the surface area of the substrate covered by the nanoparticle together with the thickness of the nanoparticle will influence the initiation of coherence to lattice misalignment and subsequent dislocation evolution. Finally, at very high negative lattice misfits [−31%; MgO/BaO(001)] even small regions of coherence are not observed. In addition, the results indicate that as the lattice misfit associated with the system increases, so the interfacial layer of the substrate becomes more defective.

For both the SrO/BaO(001) and CaO/BaO(001) systems the *average* MO distances within the plane of the interface ([100]; [010]) were 0.24 and 0.20 Å higher than MO distances perpendicular ([001]) to the interfacial plane for the SrO and CaO nanoparticles, respectively. In addition, the interplanar $MO(002)$ distances for both the SrO and CaO nanoparticles were contracted uniformly by 0.12 and 0.2 Å, respectively, suggesting the nanoparticles demonstrate anisotropy perpendicular and parallel with the interfacial plane with important implications for their properties.

ACKNOWLEDGMENTS

We would like to acknowledge funding for a 20 processor Compaq SC cluster, located at the Rutherford Appleton Laboratory, which was purchased and supported with funding from the JREI (JR99BAPAEQ) and Compaq.

*Author to whom correspondence should be addressed. Electronic address: sayle@rmcs.cramfield.ac.uk

[1] S. A. Chambers, Surf. Sci. Rep. **39**, 105 (2000).
[2] W. Lojkowski and H-J. Fecht, Prog. Mater. Sci. **45**, 339 (2000).
[3] A. P. Sutton and R. W. Balluffi, *Interfaces in Crystalline Materials*, Vol. 51 of *Monographs on the Physics and Chemistry of Materials* (Oxford University Press, New York, 1995).
[4] L. Wang and P. Clancy, Surf. Sci. **473**, 25 (2001).
[5] S. Giorgio, H. Graoui, C. Chapon, and C. R. Henry, Cryst. Res. Technol. **33**, 1061 (1998).
[6] S. Ranganathan, R. Divakar, and V. S. Raghunathan, Scr. Mater. **44**, 1169 (2001).
[7] H. V. Swygenhoven, A. Caro, and D. Farkas, Mater. Sci. Eng., A **309–310**, 440 (2001).
[8] D. J. Harris, J. H. Harding, and G. W. Watson, Acta Mater. **48**, 3039 (2000).
[9] D. C. Sayle, J. Mater. Chem. **9**, 2961 (1999).
[10] C. L. Jia, M. Siegert, and K. Urban, Acta Mater. **49**, 2783 (2001).
[11] S. R. Phillpot, P. Keblinski, D. Wolf, and F. Cleri, Interface Sci. **7**, 15 (1999).
[12] H. Pardoe, W. Chua-anusorn, T. G. St. Pierre, and J. Dobson, J. Magn. Magn. Mater. **225**, 41 (2001).
[13] J. M. Petroski, T. C. Green, and M. A. El-Sayed, J. Phys. Chem. A **105**, 5547 (2001).
[14] F. E. Kruis, H. Fissan, and A. Peled, J. Aerosol Sci. **29**, 511 (1998).
[15] M. I. Khan, J. Solid State Chem. **152**, 105 (2000).
[16] C. N. R. Rao and A. K. Cheetham, J. Mater. Chem. **11**, 2887 (2001).
[17] S. O'Brien, L. Brus, and C. B. Murray, J. Am. Chem. Soc. **123**, 12 085 (2001).
[18] A. I. Frenkel, C. W. Hills, and R. G. Nuzzo, J. Phys. Chem. B **105**, 12 689 (2001).
[19] H. Gleiter, Acta Mater. **48**, 1 (2001).
[20] J. Schiotz, F. D. Di Tolla, and K. W. Jacobsen, Nature (London) **391**, 561 (1998).
[21] D. R. Rolinson and B. Dunn, J. Mater. Chem. **11**, 963 (2001).
[22] D. C. Sayle and G. W. Watson, J. Phys. Chem. B **106**, 3916 (2002).
[23] D. C. Sayle and G. W. Watson, Phys. Chem. Chem. Phys. **2**, 5491 (2000).
[24] D. C. Sayle and G. W. Watson, Surf. Sci. **473**, 97 (2001).
[25] J. Baker and P. A. Lindgard, Phys. Rev. B **60**, 16 941 (1999).
[26] D. C. Sayle and G. W. Watson, J. Mater. Chem. **10**, 2241 (2000).
[27] D. C. Sayle and G. W. Watson, J. Phys. Chem. B **105**, 5506 (2001).
[28] S. A. Maicaneanu, D. C. Sayle, and G. W. Watson, Chem. Commun. 289 (2001).
[29] S. A. Maicaneanu, D. C. Sayle, and G. W. Watson, J. Phys. Chem. **105**, 12 481 (2001).
[30] T. X. T. Sayle, C. R. A. Catlow, D. C. Sayle, S. C. Parker, and J.

H. Harding, Philos. Mag. A **68**, 565 (1993).
[31] Philos. Mag. B **73** (1996) (special issue ''Interatomic Potentials'').
[32] P. P. Ewald, Ann. Phys. (Leipzig) **64**, 253 (1921).
[33] G. V. Lewis and C. R. A. Catlow, J. Phys. C **18**, 1149 (1985).
[34] D. C. Sayle, C. R. A. Catlow, J. H. Harding, M. J. F. Healy, S. A. Maicaneanu, S. C. Parker, B. Slater, and G. W. Watson, J. Mater. Chem. **10**, 1315 (2000).
[35] P. R. Kenway, P. M. Oliver, S. C. Parker, D. C. Sayle, T. X. T. Sayle, and J. O. Titiloye, Mol. Simul. **9**, 83 (1992).
[36] D. C. Sayle, T. X. T. Sayle, S. C. Parker, C. R. A. Catlow, and J. H. Harding, Phys. Rev. B **50**, 14 498 (1994).
[37] G. W. Watson, E. T. Kelsey, N. H. de Leeuw, D. J. Harris, and S. C. Parker, J. Chem. Soc., Faraday Trans. **92**, 433 (1996).
[38] W. Smith and T. R. Forester, *The DL_POLY* Molecular Simulation Package, URL http://www.dl.ac.uk/TCSC/Software/DL_POLY
[39] D. H. Gay and A. L. Rohl, J. Chem. Soc., Faraday Trans. **91**, 925 (1995).
[40] D. C. Sayle, C. R. A. Catlow, N. Dulamita, M. J. F. Healy, S. A. Maicaneanu, B. Slater, and G. W. Watson, Mol. Simul. **28**, 683 (2002).
[41] J. Huang and L. S. Bartell, J. Mol. Struct. **567–568**, 145 (2001).
[42] J. Wollschlager, D. Erdos, H. Goldback, R. Hopken, and K. M. Schroder, Thin Solid Films **400**, 1 (2001).
[43] P. W. Tasker and A. M. Stoneham, J. Chim. Phys. Phys.-Chim. Biol. **84**, 149 (1987).
[44] F. Ernst, A. Recnik, P. A. Langjahr, P. D. Nellist, and M. Ruhle, Acta Mater. **47**, 183 (1999).
[45] G. W. Watson, MDPREP, a computer program for the preparation and analysis of molecular dynamics simulations, 2002.
[46] D. M. Lind, S. D. Berry, G. Chern, H. Mathias, and L. R. Testardi, Phys. Rev. B **45**, 1838 (1992).
[47] M. P. Allan and D. J. Tildesley, *Computer Simulation of Liquids* (Oxford Scientific Publishing, Oxford, UK, 1987).
[48] L. Dong, J. Schnitker, R. W. Smith, and D. J. Srolovitz, J. Appl. Phys. **83**, 217 (1998).
[49] M. A. James and T. Hibma, Surf. Sci. **433-435**, 718 (1999).
[50] Y. Ashkenazy, R. S. Averback, and K. Albe, Phys. Rev. B **64**, 205409 (2001).
[51] S. H. Rhee, Y. Yang, H. S. Choi, J. H. Myoung, and K. Kim, Thin Solid Films **396**, 23 (2001).
[52] D. C. Sayle and G. W. Watson (unpublished).